HHS Public Access

Author manuscript

Retina. Author manuscript; available in PMC 2021 April 01.

Published in final edited form as:

Retina. 2020 April ; 40(4): 618–631. doi:10.1097/IAE.0000000000002657.

Subretinal drusenoid deposit in age-related macular degeneration: histologic insights into initiation, progression to atrophy, and imaging

Ling Chen, MD PhD[1,2], **Jeffrey D. Messinger, DC**[1], **Yuhua Zhang, PhD**[3], **Richard F. Spaide, MD**[4], **K. Bailey Freund, MD**[4,5,6], **Christine A. Curcio, PhD**[1]

[1]Department of Ophthalmology and Visual Sciences, School of Medicine, University of Alabama at Birmingham, Birmingham, AL, USA

[2]State Key Laboratory of Ophthalmology, Zhongshan Ophthalmic Center, Sun Yat-sen University, Guangzhou, China

[3]Doheny Eye Institute, Department of Ophthalmology, University of California - Los Angeles

[4]Vitreous Retina Macula Consultants of New York, NY, USA

[5]LuEsther T Mertz Retinal Research Center, Manhattan Eye, Ear and Throat Hospital, New York, NY, USA

[6]Department of Ophthalmology, New York University School of Medicine, New York, NY, USA.

Abstract

Purpose—To clarify the role of subretinal drusenoid deposits (SDD; pseudodrusen) in the progression of age-related macular degeneration (AMD) through high-resolution histology.

Method—In 33 eyes of 32 donors (early AMD, n=15; geographic atrophy; n=9, neovascular AMD, n=7; unremarkable, n=2), and two eyes of two donors with *in vivo* multimodal imaging including optical coherence tomography (OCT), examples of SDD contacting photoreceptors were assessed.

Results—SDD were granular extracellular deposits at the apical retinal pigment epithelium (RPE); the smallest were 4 μm wide. Outer segment (OS) fragments and RPE organelles appeared in some larger deposits. A continuum of photoreceptor degeneration included OS disruption, intrusion into inner segments (IS), and disturbance of neurosensory retina. In a transition to outer retinal atrophy, SDD appeared to shrink, OS disappeared, IS shortened, and the outer nuclear layer thinned and became gliotic. Stage 1 SDD on OCT correlated to displaced OS. Confluent and disintegrating stage 2–3 SDD on OCT and dot pseudodrusen by color fundus photography correlated to confluent deposits and ectopic RPE.

Corresponding Address: Christine A. Curcio, PhD; Department of Ophthalmology and Visual Sciences, EyeSight Foundation of Alabama Vision Research Laboratories, 1670 University Boulevard Room 360, University of Alabama at Birmingham School of Medicine, Birmingham AL 35294-0019; Phone: 205.937.3785; christinecurcio@uabmc.edu.

Conflict of Interest:

No authors report any proprietary interest.

R.F. Spaide is a consultant for Topcon Medical Systems, Genentech, and Roche and receives royalties from Topcon Medical Systems and DORC.

Conclusion—SDD may start at the RPE as granular, extracellular deposits. Photoreceptor OS, RPE organelles and cell bodies may appear in some advanced deposits. A progression to atrophy associated with deposit diminution was confirmed. Findings support a biogenesis hypothesis of outer retinal lipid cycling.

Précis

By histology, the smallest subretinal drusenoid deposits in age-related macular degeneration are granular and adjacent to the retinal pigment epithelium (RPE). The largest intrude on inner segments and may contain photoreceptor or RPE debris.

Keywords

age-related macular degeneration; autofluorescence; clinicopathologic correlation; color fundus photography; histology; optical coherence tomography; photoreceptors; retinal pigment epithelium; subretinal drusenoid deposits

Introduction

Age-related macular degeneration (AMD), a global cause of vision loss in older persons, involves loss of photoreceptors, retinal pigment epithelium (RPE), and choriocapillaris in the setting of extracellular deposits between visual cells and their blood supply. Subretinal drusenoid deposits (SDD; originally called reticular pseudodrusen), located between photoreceptors and RPE, are visualizable with optical coherence tomography (OCT).[1, 2] Although poorly represented in AMD staging systems using color fundus photography (CFP),[3, 4] SDD are now known to confer risk of progression to both atrophy and neovascularization.[5–7] Intraretinal neovascularization associates with SDD and responds to treatment, encouraging attention to SDD as a precursor sign.[8–10] SDD also signify serious vision loss, especially vision mediated by rod photoreceptors.[11–14] One of us (RFS) described an outer retinal atrophy following SDD regression[15] that included collapse of the outer nuclear layer (ONL), unclear ellipsoid zone (EZ), and thin choroid, often with intact RPE. This atrophy was proposed as a new form of advanced AMD.[16]

Three SDD stages first described in OCT imaging were further elucidated by use of adaptive optics scanning laser ophthalmoscopy (AOSLO) to disclose individual deposits and surrounding photoreceptors.[2, 17] In stage 1, a granular reflective material between the RPE and the EZ is associated with reduced reflectivity of overlying photoreceptors. In stage 2, reflective mounds elevate the EZ, and photoreceptor reflectivity is further reduced. In stage 3, SDD interrupt the EZ and appear as a reflective center surrounded by a hyporeflective annulus of degraded photoreceptors. Longitudinal examination revealed that individual SDD progressed through stages 1–3 and disappeared.[18] Patches of reflectivity above the external limiting membrane (ELM)[19, 20] over deposits were not part of the original OCT staging system but appeared in published images.[21] In a direct clinicopathologic correlation, Greferath and coworkers[20] reported that stage 3 deposits contained photoreceptor proteins and immune cells and extended through the ONL.

Questions about SDD progression of interest to clinical image interpretation include identifying histologic correlates of OCT stages 1–3 and outer retinal atrophy. How are deposits formed and cleared? What are the participating cells? How does each stage impact photoreceptors? How does the SDD staging system in OCT relate to morphologies described in CFP? [22, 23] We herein describe SDD contacting photoreceptors using high-resolution comprehensive histology to reveal all tissue components in a large sample of donor eyes, including eyes of two patients with multimodal clinical imaging during their lifetimes. We present evidence supporting clinical stages 1–3, a progression to outer retinal atrophy, and little evidence of non-local cells in SDD initiation.

Methods

Compliance

The histopathology study was approved by the institutional review board at the University of Alabama at Birmingham. Retrospective review of clinical records from two patients seen at Vitreous Retina Macula Consultants of New York was approved by the institutional review board of the Manhattan Eye, Ear, and Throat Hospital/ Northwell Health. All study components complied with the Health Insurance Portability and Accountability Act of 1996 and adhered to the tenets of the Declaration of Helsinki.

Survey of donor eyes

We utilized Project MACULA (http://www.projectmacula), an online resource of human AMD histology[24, 25] that includes systematically surveyed and photo-documented high-resolution histology of 139 maculas. Eyes were accessioned for research purposes from non-diabetic white donors to AdvancingSight (formerly the Alabama Eye Bank, Birmingham AL USA) during 1996–2012. Median death-to-preservation time was 3:49 hours (range, 0:40–11:40 hours). Ophthalmic health records were not available for most donors. Eyes with drusen[26] and geographic atrophy[27] are underrepresented in the Project MACULA resource due to specimen removal for prior studies. Neovascular AMD eyes largely predate 2006. Eyes were preserved by immersion in 1% paraformaldehyde and 2.5% glutaraldehyde in 0.1M phosphate buffer following anterior segment excision.

Tissue punches 8 mm in diameter and containing the fovea and temporal portion of the optic nerve head were post-fixed by osmium tannic acid paraphenylenediamine (OTAP) to accentuate extracellular lipid. They were embedded in epoxy resin (PolyBed 812, Polysciences, Warrington PA) for 0.8 μm-thick sections stained with 1% toluidine blue for polychromaticity.[28] At the foveal center and perifovea (2 mm superior), sections were scanned with 40X and 60X objectives (numerical aperture = 0.95 and 1.40, respectively). AMD cases were defined histologically.[29] The entry criterion for the current study was photodocumentation of SDD contacting photoreceptors. Deposits were not required to contact RPE.[29] From a sample of 72 images of SDD and photoreceptors, a progression sequence was formulated.

Assessments of SDD-photoreceptor relations are constrained by common post-mortem artifacts, yet the geometric precision of outer retinal layers also makes artifacts interpretable.

We compared photoreceptors over SDD to those not over SDD in the same section and subject to the same artifacts. These include 1) detachment of photoreceptor OS from the RPE; 2) detachment of IS at the myoid (bacillary layer detachment); [30] 3) detachment of SDD tops from their bases; 4) bowing of photoreceptors (like bananas), so that IS and OS appear continuous if sectioned along the long axis or discontinuous if sectioned across the IS and OS tips; 5) compaction, when bent OS are cut in cross-section while IS remain straight; and 6) RPE detachment from BrM at soft drusen or basal linear deposits (BLinD), a thin layer of soft druse material. We also noted Henle fiber layer (HFL) disorder and dyslamination, i.e., loss of a distinct ONL and HFL due to inward translocation of photoreceptor cell bodies. These degeneration indicators are less affected by IS and OS artefact.[31]

Clinically documented cases

Case 1: Comprehensive ophthalmologic examination including multimodal imaging was performed during a 9-year follow-up for a woman of European descent who presented at age 79 with bilateral AMD. The left eye was used for this study. Ocular history included bilateral cataract surgery. Medical history included chronic obstructive pulmonary disease (COPD), gastric cancer, and hypercholesterolemia. There was a 57 pack-year history of smoking. At presentation, inactive subretinal fibrosis was noted in the right eye. Non-exudative (subclinical)[32] type 1 macular neovascularization manifest as late staining on fluorescein angiography was present in the left eye and will be reported separately. Best-corrected visual acuity (BCVA) at baseline was 20/50 in the right eye and 20/25 in the left eye. The first near-infrared reflectance (NIR) and spectral domain OCT images (Heidelberg Spectralis HRA+OCT, Heidelberg Engineering, Heidelberg, Germany) were acquired 10 months after presentation and showed a large shallow irregular pigment epithelial detachment (PED) in the left eye without evidence of exudation. During follow-up, neither eye received treatment for neovascular AMD. At the last clinical evaluation, OCT showed no evidence of macular exudation in either eye and a persistent subfoveal shallow irregular PED in the left eye. BCVA was 20/200 in the right eye and 20/30 in the left eye. Sixteen months later, the patient died of complications of COPD at age 90 years. Eyes were recovered 6.25 hours after death by personnel of The Eye-Bank for Sight Restoration (New York USA), opened anteriorly by corneal excision, preserved by immersion in 4% phosphate buffered paraformaldehyde, and shipped overnight on wet ice to Birmingham. Descriptions of druse-associated atrophy[40] and non-exudative neovascularization for this case will be reported separately.

Case 2: Ophthalmologic examination with multimodal imaging was performed during an 11-year follow-up for a woman of European descent who presented at age 87 with advanced AMD and open angle glaucoma. Imaging included color and red-free fundus photography, fundus autofluorescence (FAF; Topcon TRC-50XF), spectral-domain OCT and NIR (Spectralis HRA+OCT). Relative to the patient's death at age 98 years, the last available FAF image was obtained at 49 months, color and red-free images were obtained at 13 months, and OCT and NIR were obtained at 8 months before death. Both eyes exhibited atrophy in association with spontaneous resolution of acquired vitelliform deposits and SDD,[33] the latter more abundant in the left than the right eye. Eyes were recovered 8.92

hours after death and processed as described above. Descriptions of outer retinal pathology in the right eye have been published.[34–36]

Results

Thirty-three eyes of 32 donors were included in the histologic survey. Donor age was 85.5 ± 5.7 years (range: 73 – 95 years), with 10 men and 22 women. Fifteen eyes had early AMD, 9 eyes had geographic atrophy, 7 eyes had neovascularization, and two were normal aged eyes.

Figure 1 shows the smallest identified SDD (4 μm x 3 μm in width and height, Figure 1A). These lesions have a granular internal structure and occupy concavities on the apical RPE surface in close contact with photoreceptor OS. Tufts of RPE apical processes with dispersed melanosomes separate individual deposits (Figure 1B) and deflect photoreceptor OS (Figure 1C). As SDD enlarge and become confluent, these tufts can disappear (Figure 1D).

Figure 2 shows a few short IS (teal arrowheads) atop individual deposits. A solitary deposit, larger than those in Figure 1, has gray granular contents and occupies a concavity extending over two adjacent RPE cells. In Figure 2A, OS status cannot be assessed due to artifactual compaction, but some IS are shorter than their neighbors. Figure 2B shows a solitary SDD under long OS, some of which are dilated and contain visible disks. Numerous OS fragments, also with visible disks (Figure 2B inset), form a cap on the SDD apex. RPE is continuous and of variable thickness.

Figure 3 shows intrusion on IS and associated ONL and HFL disturbances (Figure 3C,D). In Figure 3A the apical RPE is indented by two large neighboring solitary SDD, one with OS fragments and short overlying IS (teal arrowhead). Figure 3B shows SDD fragments under a short cone IS containing an ectopic nucleus. In Figure 3C a solitary SDD containing a few melanosomes bulges into the IS layer, and an ectopic photoreceptor nucleus localizes to the HFL, an early indication of dyslamination.[31] A noticeably dyslaminate HFL and ONL (Figure 3D) overlies a solitary SDD with OS at its apex. The RPE is continuous, thinned, and undulating.

Figure 4 shows an eye with geographic atrophy. At the atrophy border delineated by a curving ELM descent, OS are absent and IS are short (Figure 4A). SDD are set back from this border on a wavy but intact RPE layer that overlaid drusenoid material apparently lost in processing. The HFL and ONL are dyslaminate, and the HFL is disordered. At 150 μm from the ELM descent (Figure 4B) are SDD with sloughed RPE. At this location, OS and IS are longer than in Figure 4A. The HFL exhibits several ectopic nuclei, and the ONL is intact. At 400 μm from the ELM descent, the HFL is disordered with just one ectopic nucleus (Figure 4C).

Figure 5 shows a transition from SDD to outer retinal atrophy. From left to right, SDD shrink in association with photoreceptor OS displacement and IS shortening, with little variation in the thickness of RPE or BLamD. Further to the right, SDD and OS gradually disappear, IS shorten, and the ONL thins. Further still, ONL gaps due to photoreceptor loss are filled with pale-staining, hypertrophic Müller glia. The RPE remains intact over

continuous BLamD, which thickens. At the right under an upwardly deflected ELM is local RPE atrophy, with thick BLamD and large basal mounds containing granule aggregates shed from RPE. It is possible that a true ELM descent may have been present in a nearby section. We interpret this sequence as an association of SDD regression with photoreceptor degeneration, the most distinctive feature of outer retinal atrophy.

Figure 6 shows changes in the ONL suggestive of SDD clearing. Figure 6A shows SDD materials dispersed in the sub-retinal space among the photoreceptors, with some distinctive blue staining within an overlying ONL gap. IS are short, and one photoreceptor nucleus is displaced to the IS. In Figure 6B a solitary SDD closely approximates the ELM, and in an ONL gap, also recognized by its coloration, suggests either SDD material or disorganized cell processes.

Figure 7 shows histology of Case 1 with *in vivo* multimodal imaging evidence of stage 1 SDD, acquired 16 months before death. CFP shows indistinct light-yellow spots (Figure 7A), and discrete hyporeflective dot SDD appear on NIR imaging (Figure 7B). An OCT B-scan shows an extensive shallow RPE elevation with an atrophic spot nasally and very small hyperreflective deposits between ELM and RPE temporally (Figure 7C). Histology corresponds closely to the B-scan at the RPE elevation and atrophic spot (Figure 7D), instilling confidence in the identification of stage 1 SDD in the same section (Figure 7E). Heights and widths of clinically visible SDD are 10–43 μm and 11–30 μm, respectively. At higher magnification SDD are seen to be comprised of a flocculent ground substance containing an evenly spaced, granular material (Figure 7F).

Figure 8 shows multimodal *in vivo* imaging of Case 2 with confluent stage 2–3 (dot) SDD and in transition to outer retinal atrophy. FAF, red-free, CFP, and NIR images from 49, 13, 13, and 8 months before death, respectively (Figure 8A–D), together show hyperautofluorescent vitelliform lesions that converted to multilobular geographic atrophy, in association with hyperpigmentation. Images also show classic reticular pseudodrusen especially in superior macula, evident as numerous dot SDD that are yellow (CFP), hypoautofluorescent (FAF) and hyporeflective (NIR), the latter with a target configuration.[19] OCT scans (Figure 8E,F) show disintegrating stage 3 deposits and marked loss of outer retinal architecture. The EZ is poorly visualized, the IZ is invisible, and the HFL-ONL is thinned. Figure 8E shows material accumulated between individual SDD. Figure 8F does not show ELM, EZ, or IZ.

Figure 9 shows histology of Case 2. This eye had hard drusen, parafoveal areas of atrophy delimited by ELM descents, and thick basal laminar deposit overlying thin BLinD (Figure 9B, orange inset and arrowheads), without evidence of neovascularization. In Figure 9A, three undulating SDD are detached from a fourth SDD (on the left) and from the RPE (in the center). Photoreceptor OS are shortened but IS are intact, supporting designation of these deposits as stage 2 (Figure 9A). Near an area of atrophic RPE (Figure 9B), SDD fragments can be observed in the sub-retinal space under an elevated but intact ELM. In this area, OS are absent and IS are short, consistent with stage 3 SDD. Deposits contain several ovoid, fully granulated sloughed RPE. The underlying RPE is variable in thickness. Some Intraretinal RPE in the area of HFL/ONL dyslamination (Figure 9B, inserts) had irregular

somata and large bronze-staining pigment granules like those in the RPE layer. Others had an ovoid soma and smaller greenish-staining granules with melanosomes.

Discussion

Our histologic survey and clinicopathologic correlation revealed the earliest SDD stages seen to date. Further, we observed a progression from SDD to outer retinal atrophy consistent with the original clinical description.[15] Our data provide insight into the composition, biogenesis, lifecycle, and clinical imaging correlates of SDD.

This report built upon prior histology and an understanding of image formation mechanisms in OCT and AOSLO. Previous research had identified SDD as dollops or mounds of a granular extracellular material interspersed with tufts of RPE apical processes.[29, 37–40] This material contained histochemically detectable unesterified cholesterol, apolipoprotein E, vitronectin, complement factor H, and CD59.[20, 38, 40–42] Image formation involves photoreceptor waveguiding properties, photoreceptor orientation and directionality, and light scattering from water-lipid interfaces.[25, 43] The inhomogeneous ultrastructure of SDD, attributable to lipid embedded in a proteinaceous material,[38–41] could impart a granular hyperreflectivity.[44] Stages 1–3 defined in OCT and refined in AOSLO were conceived, in turn, as deposits of increasing size bending or shortening photoreceptor OS, displacing OS and shortening IS, and intruding into the IS layer, with OS deflection or loss. Reflectivity internal to the ELM could be deposit material,[21] reactive gliosis,[45] disorder of the HFL,[31] or some combination.

Regarding composition, the smallest SDD had an evenly spaced, finely granular material dispersed within a flocculent ground substance, consistent with evidence for particulate membranous profiles [2, 37–39] containing lipid.[41] In this expanded sample, we also observed that some deposits were capped by OS fragments with disks (Figures 2B, 3D; see also Figure 4A, 5D [29]) when overlying photoreceptors are degenerated, i.e., late in the deposit lifecycle. Stage-specific compositional evolution helps explain reports of both absence[38] and presence[20] of opsin immunoreactivity, and OS-like structures lacking obvious disks. [29, 46] Our data, with others,[33] do not support conclusions that SDD are “degenerating photoreceptor cells”[47] or “not phagocytosed OS”.[19] Some stage 3 deposits contained scattered RPE organelles (Figure 3C), consistent with RPE degranulation as a degeneration pathway.[48, 49] These were infrequent, explaining why SDD are generally considered hypoautofluorescent.[50, 51] Intriguingly, others have reported small features on the apical surface of normal RPE that are immunoreactive for the amino acid taurine and complement receptor 1 /CD35.[52, 53] Whether these structures evolve into SDD merits investigation.

A virtual absence of immune cells in or near SDD was surprising due to findings in both humans and mouse models. Greferath et al reported cells expressing ionized calcium binding adaptor molecule 1, i.e., either microglia or macrophages, adhered to stage 3 deposits.[20] Microglia migrate from inner to outer retina in diverse photoreceptor degenerations, including advanced AMD.[31, 54–59] However, these were not detected in our sample of mostly stage 1–2 lesions, paralleling the sparse cells seen in smaller deposits of the Greferath et al specimen (E.L. Fletcher & U Greferath personal communication, 6/11/2019).

Paucity of immune cells in the subretinal space contrasts with the sub-RPE-basal laminar space, where cells (some RPE-derived) occupy at least 13% of sampled locations in advanced AMD eyes.[31, 58] It also contrasts with atheroma which characteristically includes immune cells.[59] One possible explanation is that lipid-rich drusen and atheroma generate more peroxidizable and pro-inflammatory lipids to recruit such cells than does SDD. Also, the sub-RPE-basal laminar space is accessible to the systemic circulation unlike the subretinal space. Subretinal phagocytes clear excess neurons during human fetal development, [60, 61] but similar cells in normal aged maculas have not been detected to date (unpublished observations, n= 60, Project MACULA website; CAC). Our findings in human AMD contrast with those in mouse models, including aged wild-type animals, in which resident microglia populate the subretinal space.[62–68] These species differences are relevant to the interpretation of pre-clinical data.

Our data bear on mechanisms of SDD clearance. Greferath et al[20] demonstrated a continuity of vitronectin-immunoreactive SDD with similar material in the ONL. In our previous[38] and current histology (Figure 6), distinct staining and texture within ONL gaps overlying SDD may be deposit material positioned for clearing, cellular processes (e.g., reactive Müller glia) or both. A proposed stage 4 of resorption and clearance[21] included hyperreflective material above the ELM and highly reflective spherical features suggestive of anteriorly migrating RPE (see Figure 9). This prior study predated histologic validation of hyperreflective foci in AMD as RPE and non-RPE.[36, 69, 70]

We propose that Figure 5 correlates to outer retinal atrophy,[15] as SDD disappearance was linked with progression indicators, including thickened basal laminar deposit and reactive gliosis, with minimal RPE atrophy. Outer retinal atrophy was defined as a distinct end-stage of AMD with an intact RPE layer. Notably, in Figure 5 photoreceptors are long where individual SDD are large, and as photoreceptors degenerate, deposits shrink. Recently, we[15] and others [20] demonstrated in areas clinically suggestive of SDD regression, photoreceptor shortening and RPE dysmorphia.[71] These observations support a hypothesis, developed for drusen,[72] that outer retinal cells must be functional to form, grow, and maintain extracellular deposits. Conversely, deposit disappearance is not beneficial if it means that contributory cells deteriorated. The RPE, metabolic gatekeeper for photoreceptors,[73] may persist during outer retinal atrophy, because of proximity to the choriocapillaris, whereas photoreceptors decline, due to distance. We note that progression to atrophy including an ELM descent towards BrM, a component of drusen-associated atrophy signifying Müller cell activity, was seen in two instances (Figures 4, 9). Because these regions also contained soft drusen, it remains to be determined if an ELM descent occurs where only SDD are present. Interestingly, eyes with SDD did not exhibit a glial seal, i.e., penetration of reactive Müller glia into the sub-RPE-BL space,[70, 74, 75] perhaps reflecting healthier RPE in eyes with SDD relative to drusen.

Our exploration was guided by a theory of AMD deposit pathogenesis that encompasses both SDD and soft drusen/ BLinD. As reviewed [7, 76, 77] (also Supplementary Table), this theory holds that deposits represent dysregulation of constitutive lipid transfer and cycling pathways required by the specialized physiologies of rods and cones, with the participation of RPE, Müller glia, and choriocapillary endothelium. Supporting this concept is the distinct

lipid composition and topographies of SDD and soft drusen, which resemble that of rods[29, 51, 78–81] and cones, respectively.[20, 38, 40] Drusen form, because functional RPE constitutively secretes large lipoprotein particles throughout adulthood that fill BrM, as translocation across the BrM–ChC complex is impaired age-dependently.[76, 82, 83] Drusen grow because normally secreted RPE products are cleared inefficiently, and they collapse after RPE migration or death terminates production.[15, 72, 84, 85] Proposed molecular mechanisms underlying SDD [7, 29, 77] involve protein-mediated transfer of unesterified cholesterol, fatty acids, retinoids, and xanthophyll carotenoids. Recent experimental studies show that lipid pathways known from liver and intestine also intersect in outer retina, lend credence to the existence of multifunctional carriers required by this theory. [86, 87]

Within this framework, our data inform an SDD lifecycle of growth and regression (Figure 10). The smallest SDD are found at the RPE, suggesting that they start there. Given continuous transport cycles among outer retinal cells, we propose that a molecular blockage at the RPE, for example, a failure to bind or uptake cycled lipids, could lead to accumulated materials. We further suggest that once begun, a deposit seeds the physical accumulation of subsequent material from the top, like a midden, including OS fragments in some instances. Our findings support deposit growth upwards towards the ELM, as photoreceptors focally shorten, and eventually clearance by Müller glia through the retina. Some RPE-photoreceptor exchange likely continues at the long apical processes contacting cones, before deposits become confluent.[88] An initial blockage at the photoreceptors is theoretically possible but is also more complex. Clearly these ideas need rigorous testing by methods outside our current scope.

Knowing the limits of SDD clinical visibility can help trial design. One tested therapy exacerbated progression in eyes with SDD,[89] and such eyes might be excluded from future trials if SDD were reliably visible. Previous comparisons of *en face* SDD imaging and histology had mixed and sometimes conflicting results.[2, 20, 29, 38, 39] We found a morphologic continuum comparable with OCT, with successively greater intrusion of SDD into the IS layer followed by ONL and HFL disturbance. By direct clinicopathologic correlation (Figure 7), deposits at stage 1 (11–30 μm wide and 10–43 μm tall) are poorly visible by CFP (compare to drusen, which are visible at 30 μm diameter[90]). In an eye with dot SDD on CFP and disintegrating stages 2–3 on OCT (Figure 8), histology showed confluent SDD up to 64 μm tall, suggesting that only deposit tips are visible in CFP.

Strengths of this report are a systematic review of many donor eyes at short death-to-preservation interval, two eyes with excellent *in vivo* multimodal imaging, comprehensive, high-resolution histology and microscopy, and a theoretical framework for deposit biogenesis well supported in human biology. Limitations are detachments and study design that prevented integration across all relevant tissue layers, biases in the donor eye sample, lack of molecular identifications due to glutaraldehyde fixation, lack of serial sections to disambiguate off-axis cuts, and the subjective nature of histology. Despite these shortcomings, this is the largest number of eyes surveyed to date for SDD, and many correspondences to clinical imaging were found. Many questions raised by these data, in particular cross-layer integration, are addressable by viewing individual deposits over time in intact living eyes.[18] Given the ample evidence that SDD progress to atrophy and

neovascularization (Supplementary Table), our data strongly support including SDD as a diagnostic criterion for AMD. Indeed, a histologic definition of AMD (severe RPE change in the setting of drusen/ BLinD),[91] expanded to include SDD, could be considered as an OCT definition of AMD. Encouraged by recent progress in understanding and targeting soft drusen for therapeutic purposes, we offer these data to guide research towards similar advances for SDD.

Supplementary Material

Refer to Web version on PubMed Central for supplementary material.

Acknowledgments

We thank the Alabama Eye Bank (Birmingham AL) and the Eye-Bank for Sight Restoration (New York) for timely retrieval of donor eyes and David Fisher for graphic design of Figure 10.

Financial support:

This work was supported by The Macula Foundation, New York, the John P. and Shirley H. Sarks Fund at UAB, and Heidelberg Engineering. The Project MACULA website and the recovery of human donor eyes for research has been supported by NIH grant R01EY06019, EyeSight Foundation of Alabama, International Retinal Research Foundation, Edward N. and Della L. Thome Foundation, the Arnold and Mabel Beckman Initiative for Macular Research, and Research to Prevent Blindness. Purchase of the slide scanner was made possible by the Carl G. and Pauline Buck Trust. Yuhua Zhang was supported by the NIH grant R01EY024378.

K.B. Freund is a consultant for Optovue, Heidelberg Engineering, Allergan, Zeiss, Novartis, and Genentech and receives research support from Genentech/Roche.

C.A. Curcio receives research funding from Heidelberg Engineering and Genentech/Roche.

References

1. Zweifel SA, Imamura Y, Spaide TC et al. Prevalence and significance of subretinal drusenoid deposits (reticular pseudodrusen) in age-related macular degeneration. Ophthalmology 2010; 117:1775–1781. [PubMed: 20472293]
2. Zweifel SA, Spaide RF, Curcio CA et al. Reticular pseudodrusen are subretinal drusenoid deposits. Ophthalmology 2010; 117:303–312 e301. [PubMed: 19815280]
3. Klein R, Davis MD, Magli YL et al. The wisconsin age-related maculopathy grading system. Ophthalmology 1991; 98:1128–1134. [PubMed: 1843453]
4. Ferris FL 3rd, Wilkinson CP, Bird A et al. Clinical classification of age-related macular degeneration. Ophthalmology 2013; 120:844–851. [PubMed: 23332590]
5. Marsiglia M, Boddu S, Bearelly S et al. Association between geographic atrophy progression and reticular pseudodrusen in eyes with dry age-related macular degeneration. Invest Ophthalmol Vis Sci 2013; 54:7362–7369. [PubMed: 24114542]
6. Steinberg JS, Gobel AP, Fleckenstein M et al. Reticular drusen in eyes with high-risk characteristics for progression to late-stage age-related macular degeneration. Br J Ophthalmol 2015; 99:1289–1294. [PubMed: 25795913]
7. Spaide RF, Ooto S and Curcio CA. Subretinal drusenoid deposits AKA pseudodrusen. Surv Ophthalmol 2018; 63:782–815. [PubMed: 29859199]
8. Su D, Lin S, Phasukkijwatana N et al. An updated staging system of type 3 neovascularization using spectral domain optical coherence tomography. Retina 2016; 36 Suppl 1:S40–S49. [PubMed: 28005662]
9. Sawa M, Ueno C, Gomi F and Nishida K. Incidence and characteristics of neovascularization in fellow eyes of Japanese patients with unilateral retinal angiomatous proliferation. Retina 2014; 34:761–767. [PubMed: 24100709]

10. Nagiel A, Sarraf D, Sadda SR et al. Type 3 neovascularization: evolution, association with pigment epithelial detachment, and treatment response as revealed by spectral domain optical coherence tomography. Retina 2015; 35:638–647. [PubMed: 25650713]
11. Flamendorf J, Agron E, Wong WT et al. Impairments in dark adaptation are associated with age-related macular degeneration severity and reticular pseudodrusen. Ophthalmology 2015; 122:2053–2062. [PubMed: 26253372]
12. Flynn OJ, Cukras CA and Jeffrey BG. Characterization of rod function phenotypes across a range of age-related macular degeneration severities and subretinal drusenoid deposits. Invest Ophthalmol Vis Sci 2018; 59:2411–2421. [PubMed: 29847647]
13. Steinberg JS, Fitzke FW, Fimmers R et al. Scotopic and photopic microperimetry in patients with reticular drusen and age-related macular degeneration. JAMA Ophthalmol 2015; 133:690–697. [PubMed: 25811917]
14. Chen KG, Alvarez JA, Yazdanie M et al. Longitudinal study of dark adaptation as a functional outcome measure for age-related macular degeneration. Ophthalmology 2019; 126:856–865. [PubMed: 30278196]
15. Spaide RF. Outer retinal atrophy after regression of subretinal drusenoid deposits as a newly recognized form of late age-related macular degeneration. Retina 2013; 33:1800–1808. [PubMed: 23764969]
16. Spaide RF. Improving the age-related macular degeneration construct: a new classification system. Retina 2018; 38:891–899. [PubMed: 28557901]
17. Zhang Y, Wang X, Rivero EB et al. Photoreceptor perturbation around subretinal drusenoid deposits as revealed by adaptive optics scanning laser ophthalmoscopy. Am J Ophthalmol 2014; 158:584–596 e581. [PubMed: 24907433]
18. Zhang Y, Wang X, Godara P et al. Dynamism of dot subretinal drusenoid deposits in age-related macular degeneration demonstrated with adaptive optics imaging. Retina 2018; 38:29–38. [PubMed: 28196054]
19. Querques G, Querques L, Martinelli D et al. Pathologic insights from integrated imaging of reticular pseudodrusen in age-related macular degeneration. Retina 2011; 31:518–526. [PubMed: 21150696]
20. Greferath U, Guymer RH, Vessey KA et al. Correlation of histologic features with in vivo imaging of reticular pseudodrusen. Ophthalmology 2016; 123:1320–1331. [PubMed: 27039021]
21. Querques G, Canoui-Poitrine F, Coscas F et al. Analysis of progression of reticular pseudodrusen by spectral domain-optical coherence tomography. Invest Ophthalmol Vis Sci 2012; 53:1264–1270. [PubMed: 22266524]
22. Suzuki M, Sato T and Spaide RF. Pseudodrusen subtypes as delineated by multimodal imaging of the fundus. Am J Ophthalmol 2014; 157:1005–1012. [PubMed: 24503406]
23. Zhou Q, Daniel E, Maguire MG et al. Pseudodrusen and Incidence of Late Age-Related Macular Degeneration in Fellow Eyes in the Comparison of Age-Related Macular Degeneration Treatments Trials. Ophthalmology 2016; 123:1530–1540. [PubMed: 27040149]
24. Curcio CA, Zanzottera EC, Ach T et al. Activated retinal pigment epithelium, an optical coherence tomography biomarker for progression in age-related macular degeneration. Invest Ophthalmol Vis Sci 2017; 58:BIO211–BIO226. [PubMed: 28785769]
25. Dolz-Marco R, Glover JP, Gal-Or O et al. Choroidal and sub-retinal pigment epithelium caverns: multimodal imaging and correspondence with friedman lipid globules. Ophthalmology 2018; 125:1287–1301. [PubMed: 29625839]
26. Rudolf M, Clark ME, Chimento MF et al. Prevalence and morphology of druse types in the macula and periphery of eyes with age-related maculopathy. Invest Ophthalmol Vis Sci 2008; 49:1200–1209. [PubMed: 18326750]
27. Rudolf M, Vogt SD, Curcio CA et al. Histologic basis of variations in retinal pigment epithelium autofluorescence in eyes with geographic atrophy. Ophthalmology 2013; 120:821–828. [PubMed: 23357621]
28. Curcio CA, Messinger JD, Sloan KR et al. Human chorioretinal layer thicknesses measured in macula-wide, high-resolution histologic sections. Invest Ophthalmol Vis Sci 2011; 52:3943–3954. [PubMed: 21421869]

29. Curcio CA, Messinger JD, Sloan KR et al. Subretinal drusenoid deposits in non-neovascular age-related macular degeneration: morphology, prevalence, topography, and biogenesis model. Retina 2013; 33:265–276. [PubMed: 23266879]
30. Mehta N, Chong J, Tsui E et al. Presumed foveal bacillary layer detachment in a patient with toxoplasmosis chorioretinitis and pachychoroid disease. Retin Cases Brief Rep 2018.
31. Li M, Huisingh C, Messinger J et al. Histology of geographic atrophy secondary to age-related macular degeneration: a multilayer approach. Retina 2018; 38:1937–1953. [PubMed: 29746415]
32. de Oliveira Dias JR, Zhang Q, Garcia JMB et al. Natural history of subclinical neovascularization in nonexudative age-related macular degeneration using swept-source OCT angiography. Ophthalmology 2018; 125:255–266. [PubMed: 28964581]
33. Spaide RF, Yannuzzi L, Freund KB et al. Eyes with subretinal drusenoid deposits and no drusen: progression of macular findings. Retina 2019; 39:12–26. [PubMed: 30312263]
34. Litts KM, Messinger JD, Dellatorre K et al. Clinicopathological correlation of outer retinal tubulation in age-related macular degeneration. JAMA Ophthalmol 2015; 133:609–612. [PubMed: 25742505]
35. Dolz-Marco R, Balaratnasingam C, Messinger JD et al. The border of macular atrophy in age-related macular degeneration: a clinicopathologic correlation. Am J Ophthalmol 2018; 193:166–177. [PubMed: 29981740]
36. Zanzottera EC, Messinger JD, Ach T et al. The project MACULA retinal pigment epithelium grading system for histology and optical coherence tomography in age-related macular degeneration. Invest Ophthalmol Vis Sci 2015; 56:3253–3268. [PubMed: 25813989]
37. Sarks JP, Sarks SH and Killingsworth MC. Evolution of geographic atrophy of the retinal pigment epithelium. Eye (Lond) 1988; 2 (Pt 5):552–577. [PubMed: 2476333]
38. Rudolf M, Malek G, Messinger JD et al. Sub-retinal drusenoid deposits in human retina: organization and composition. Exp Eye Res 2008; 87:402–408. [PubMed: 18721807]
39. Sarks J, Arnold J, Ho IV et al. Evolution of reticular pseudodrusen. Br J Ophthalmol 2011; 95:979–985. [PubMed: 21109695]
40. Curcio CA, Presley JB, Malek G et al. Esterified and unesterified cholesterol in drusen and basal deposits of eyes with age-related maculopathy. Exp Eye Res 2005; 81:731–741. [PubMed: 16005869]
41. Oak AS, Messinger JD and Curcio CA. Subretinal drusenoid deposits: further characterization by lipid histochemistry. Retina 2014; 34:825–826. [PubMed: 24589874]
42. Ebrahimi KB, Fijalkowski N, Cano M and Handa JT. Decreased membrane complement regulators in the retinal pigmented epithelium contributes to age-related macular degeneration. J Pathol 2013; 229:729–742. [PubMed: 23097248]
43. Litts KM, Zhang Y, Freund KB and Curcio CA. Optical coherence tomography and histology of age-related macular degeneration support mitochondria as reflectivity sources. Retina 2018; 38:445–461. [PubMed: 29210936]
44. Meadway A, Wang X, Curcio CA and Zhang Y. Microstructure of subretinal drusenoid deposits revealed by adaptive optics imaging. Biomed Opt Express 2014; 5:713–727. [PubMed: 24688808]
45. Tan ACS, Astroz P, Dansingani KK et al. The evolution of the plateau, an optical coherence tomography signature seen in geographic atrophy. Invest Ophthalmol Vis Sci 2017; 58:2349–2358. [PubMed: 28437524]
46. Arnold JJ, Sarks JP, Killingsworth MC et al. Adult vitelliform macular degeneration: a clinicopathological study. Eye (Lond) 2003; 17:717–726. [PubMed: 12928683]
47. Paavo M, Lee W, Merriam J et al. Intraretinal correlates of reticular pseudodrusen revealed by autofluorescence and en face oct. Invest Ophthalmol Vis Sci 2017; 58:4769–4777. [PubMed: 28973322]
48. Ach T, Tolstik E, Messinger JD et al. Lipofuscin redistribution and loss accompanied by cytoskeletal stress in retinal pigment epithelium of eyes with age-related macular degeneration. Invest Ophthalmol Vis Sci 2015; 56:3242–3252. [PubMed: 25758814]
49. Gambril JA, Sloan KR, Swain TA et al. Quantifying retinal pigment epithelium dysmorphia and loss of histologic autofluorescence in age-related macular degeneration. Invest Ophthalmol Vis Sci 2019; 60:2481–2493. [PubMed: 31173079]

50. Lee MY and Ham DI. Subretinal drusenoid deposits with increased autofluorescence in eyes with reticular pseudodrusen. Retina 2014; 34:69–76. [PubMed: 23743636]
51. Zarubina AV, Neely DC, Clark ME et al. Prevalence of subretinal drusenoid deposits in older persons with and without age-related macular degeneration, by multimodal imaging. Ophthalmology 2016; 123:1090–1100. [PubMed: 26875000]
52. Jones BW, Pfeiffer RL, Ferrell WD et al. Retinal remodeling and metabolic alterations in human AMD. Front Cell Neurosci 2016; 10:103. [PubMed: 27199657]
53. Fett AL, Hermann MM, Muether PS et al. Immunohistochemical localization of complement regulatory proteins in the human retina. Histol Histopathol 2012; 27:357–364. [PubMed: 22237713]
54. Di Pierdomenico J, Garcia-Ayuso D, Agudo-Barriuso M et al. Role of microglial cells in photoreceptor degeneration. Neural Regen Res 2019; 14:1186–1190. [PubMed: 30804243]
55. Rashid K, Wolf A and Langmann T. Microglia activation and immunomodulatory therapies for retinal degenerations. Front Cell Neurosci 2018; 12:176. [PubMed: 29977192]
56. Gupta N, Brown KE and Milam AH. Activated microglia in human retinitis pigmentosa, late-onset retinal degeneration, and age-related macular degeneration. Exp Eye Res 2003; 76:463–471. [PubMed: 12634111]
57. Lad EM, Cousins SW, Van Arnam JS and Proia AD. Abundance of infiltrating CD163+ cells in the retina of postmortem eyes with dry and neovascular age-related macular degeneration. Graefes Arch Clin Exp Ophthalmol 2015; 253:1941–1945. [PubMed: 26148801]
58. Zanzottera EC, Messinger JD, Ach T et al. Subducted and melanotic cells in advanced age-related macular degeneration are derived from retinal pigment epithelium. Invest Ophthalmol Vis Sci 2015; 56:3269–3278. [PubMed: 26024109]
59. Tabas I, Garcia-Cardena G and Owens GK. Recent insights into the cellular biology of atherosclerosis. J Cell Biol 2015; 209:13–22. [PubMed: 25869663]
60. McMenamin PG and Loeffler KU. Cells resembling intraventricular macrophages are present in the subretinal space of human foetal eyes. Anat Rec 1990; 227:245–253. [PubMed: 2350012]
61. McMenamin PG, Saban DR and Dando SJ. Immune cells in the retina and choroid: Two different tissue environments that require different defenses and surveillance. Prog Retin Eye Res 2018.
62. Combadiere C, Feumi C, Raoul W et al. CX3CR1-dependent subretinal microglia cell accumulation is associated with cardinal features of age-related macular degeneration. J Clin Invest 2007; 117:2920–2928. [PubMed: 17909628]
63. Raoul W, Feumi C, Keller N et al. Lipid-bloated subretinal microglial cells are at the origin of drusen appearance in CX3CR1-deficient mice. Ophthalmic Res 2008; 40:115–119. [PubMed: 18421223]
64. Xu H, Chen M, Manivannan A et al. Age-dependent accumulation of lipofuscin in perivascular and subretinal microglia in experimental mice. Aging Cell 2008; 7:58–68. [PubMed: 17988243]
65. Xu H, Chen M and Forrester JV. Para-inflammation in the aging retina. Prog Retin Eye Res 2009; 28:348–368. [PubMed: 19560552]
66. Ma W, Zhao L, Fontainhas AM et al. Microglia in the mouse retina alter the structure and function of retinal pigmented epithelial cells: a potential cellular interaction relevant to AMD. PLoS One 2009; 4:e7945. [PubMed: 19936204]
67. Chen M, Forrester JV and Xu H. Dysregulation in retinal para-inflammation and age-related retinal degeneration in CCL2 or CCR2 deficient mice. PLoS One 2011; 6:e22818. [PubMed: 21850237]
68. Ban N, Lee TJ, Sene A et al. Impaired monocyte cholesterol clearance initiates age-related retinal degeneration and vision loss. JCI Insight 2018; 3.
69. Balaratnasingam C, Messinger JD, Sloan KR et al. Histologic and optical coherence tomographic correlates in drusenoid pigment epithelium detachment in age-related macular degeneration. Ophthalmology 2017; 124:644–656. [PubMed: 28153442]
70. Li M, Dolz-Marco R, Messinger JD et al. Clinicopathologic correlation of anti-vascular endothelial growth factor-treated type 3 neovascularization in age-related macular degeneration. Ophthalmology 2018; 125:276–287. [PubMed: 28964579]
71. Li M, Dolz-Marco R, Huisingh C et al. Clinicopathologic correlation of geographic atrophy secondary to age-related macular degeneration. Retina 2019; 39:802–816. [PubMed: 30839495]

72. Balaratnasingam C, Yannuzzi LA, Curcio CA et al. Associations between retinal pigment epithelium and drusen volume changes during the lifecycle of large drusenoid pigment epithelial detachments. Invest Ophthalmol Vis Sci 2016; 57:5479–5489. [PubMed: 27760262]
73. Kanow MA, Giarmarco MM, Jankowski CS et al. Biochemical adaptations of the retina and retinal pigment epithelium support a metabolic ecosystem in the vertebrate eye. Elife 2017; 6.
74. Curcio CA, Medeiros NE and Millican CL. Photoreceptor loss in age-related macular degeneration. Invest Ophthalmol Vis Sci 1996; 37:1236–1249. [PubMed: 8641827]
75. Anderson DH, Guerin CJ, Erickson PA et al. Morphological recovery in the reattached retina. Invest Ophthalmol Vis Sci 1986; 27:168–183. [PubMed: 3943943]
76. Curcio CA. Soft drusen in age-related macular degeneration: biology and targeting via the oil spill strategies. Invest Ophthalmol Vis Sci 2018; 59:AMD160–AMD181. [PubMed: 30357336]
77. Curcio CA. Antecedents of soft drusen, the specific deposits of age-related macular degeneration, in the biology of human macula. Invest Ophthalmol Vis Sci 2018; 59:AMD182–AMD194. [PubMed: 30357337]
78. Curcio CA, Sloan KR, Kalina RE and Hendrickson AE. Human photoreceptor topography. J Comp Neurol 1990; 292:497–523. [PubMed: 2324310]
79. Steinberg JS, Auge J, Jaffe GJ et al. Longitudinal analysis of reticular drusen associated with geographic atrophy in age-related macular degeneration. Invest Ophthalmol Vis Sci 2013; 54:4054–4060. [PubMed: 23633663]
80. Wang JJ, Rochtchina E, Lee AJ et al. Ten-year incidence and progression of age-related maculopathy: the blue Mountains Eye Study. Ophthalmology 2007; 114:92–98. [PubMed: 17198852]
81. Yehoshua Z, Wang F, Rosenfeld PJ et al. Natural history of drusen morphology in age-related macular degeneration using spectral domain optical coherence tomography. Ophthalmology 2011; 118:2434–2441. [PubMed: 21724264]
82. Johnson PT, Lewis GP, Talaga KC et al. Drusen-associated degeneration in the retina. Invest Ophthalmol Vis Sci 2003; 44:4481–4488. [PubMed: 14507896]
83. Johnson PT, Brown MN, Pulliam BC et al. Synaptic pathology, altered gene expression, and degeneration in photoreceptors impacted by drusen. Invest Ophthalmol Vis Sci 2005; 46:4788–4795. [PubMed: 16303980]
84. Pilgrim MG, Lengyel I, Lanzirotti A et al. Subretinal pigment epithelial deposition of drusen components including hydroxyapatite in a primary cell culture model. Invest Ophthalmol Vis Sci 2017; 58:708–719. [PubMed: 28146236]
85. Scoles D, Sulai YN, Cooper RF et al. Photoreceptor inner segment morphology in best vitelliform macular dystrophy. Retina 2017; 37:741–748. [PubMed: 27467379]
86. Shyam R, Gorusupudi A, Nelson K et al. RPE65 has an additional function as the lutein to meso-zeaxanthin isomerase in the vertebrate eye. Proc Natl Acad Sci U S A 2017; 114:10882–10887. [PubMed: 28874556]
87. Storti F, Klee K, Todorova V et al. Impaired ABCA1/ABCG1-mediated lipid efflux in the mouse retinal pigment epithelium (RPE) leads to retinal degeneration. Elife 2019; 8.
88. Krebs W and Krebs I. Primate retina and choroid. Springer-Verlag New York, 1991.
89. Guymer RH, Wu Z, Hodgson LAB et al. Subthreshold nanosecond laser intervention in age-related macular degeneration: the lead randomized controlled clinical trial. Ophthalmology 2019; 126:829–838. [PubMed: 30244144]
90. Rudolf M, Seckerdieck K, Grisanti S and Curcio CA. Internal structure consistent with remodelling in very small drusen, revealed by filipin histochemistry for esterified cholesterol. Br J Ophthalmol 2014; 98:698–702. [PubMed: 24554738]
91. Curcio CA, Medeiros NE and Millican CL. The alabama age-related macular degeneration grading system for donor eyes. Invest Ophthalmol Vis Sci 1998; 39:1085–1096. [PubMed: 9620067]

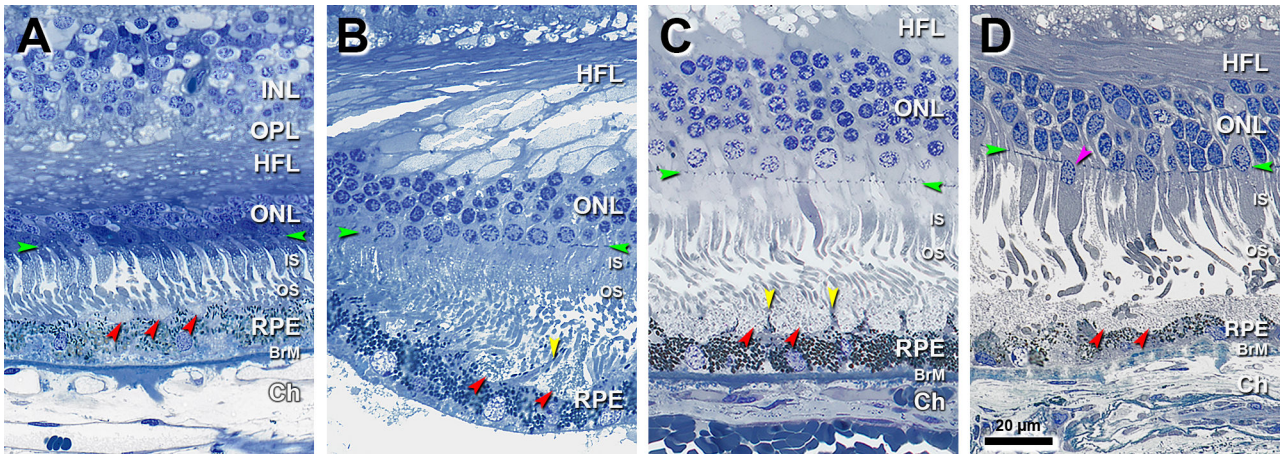

Figure 1. Small deposits separated by apical processes become confluent.

INL, inner nuclear layer; OPL, outer plexiform layer; HFL, Henle fiber layer; ONL, outer nuclear layer; IS, inner segment; OS, outer segment; RPE, retinal pigment epithelium; BrM, Bruch membrane; Ch, choroid; Green arrowheads, external limiting membrane. Red arrowheads, SDD, subretinal drusenoid deposits. Scale bar in (D) applies to all panels. Post-mortem compaction artifact is visible in A-C. **A.** 950 µm temporal. Three small SDD are located on the apical of RPE, with corresponding concavities in the apical surface of the RPE. Photoreceptor OS are deflected by the deposits and bent due to post-mortem artefactual compaction. Melanosomes can be observed within apical processes. Eighty-year-old man. **B.** 1200 µm temporal. Two small SDD separated by RPE apical process (yellow arrowhead). Photoreceptor OS are deflected by the SDD. RPE was detached from BrM at a soft druse, which is almost empty. Seventy-three-year-old woman. **C.** 1900 µm nasal. SDD are confluent. Tufts of apical processes are still visible (yellow arrowhead). Photoreceptor OS are deflected. Eighty-year-old man. **D.** 2800 µm nasal. SDD are confluent, with bent and shed OS. Apical processes are not visible. Ectopic photoreceptor nucleus in IS (purple arrowhead). Eighty-five-year-old woman.

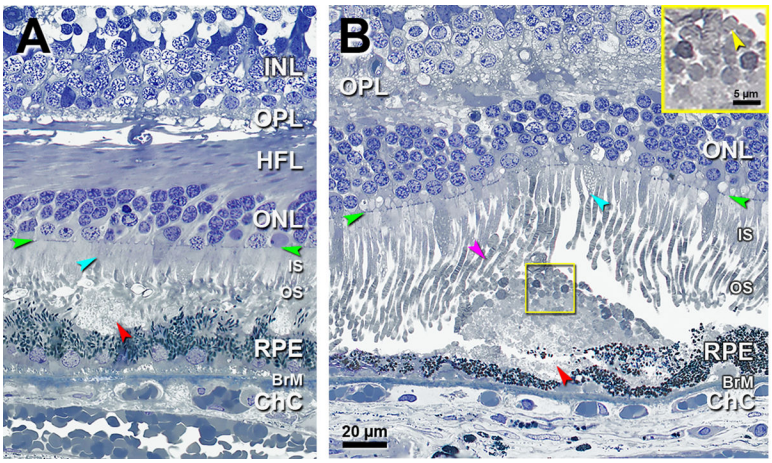

Figure 2. Solitary SDD affect overlying inner segments and may have outer segment debris.
INL, inner nuclear layer; OPL, outer plexiform layer; HFL, Henle fiber layer; ONL, outer nuclear layer; IS, inner segment; OS, outer segment; RPE, retinal pigment epithelium; BrM, Bruch membrane; Green arrowheads, ELM, external limiting membrane; Red arrowheads, SDD, subretinal drusenoid deposits. Scale bar in (B) applies to all panels. **A.** 900 µm temporal. A solitary mound of SDD is located in the sub-retinal space. Due to artefactual compaction, OS are seen as cross-sections. OS are reduced on top of the SDD (compare to OS at the right of the SDD). Some photoreceptor IS are short (teal arrowhead). Eighty-three-year-old woman. **B.** 1800 µm nasal A large solitary mound of SDD is located above RPE of very non-uniform thickness. Photoreceptors OS are short on the top of SDD and deflected by SDD (purple arrowhead), with visible disks. Numerous photoreceptor OS remains, some with disks, form a cap on the surface of the SDD (yellow frame, also yellow inset and yellow arrowhead). Some photoreceptor IS are short (teal arrowhead). Eighty-six-year-old man.

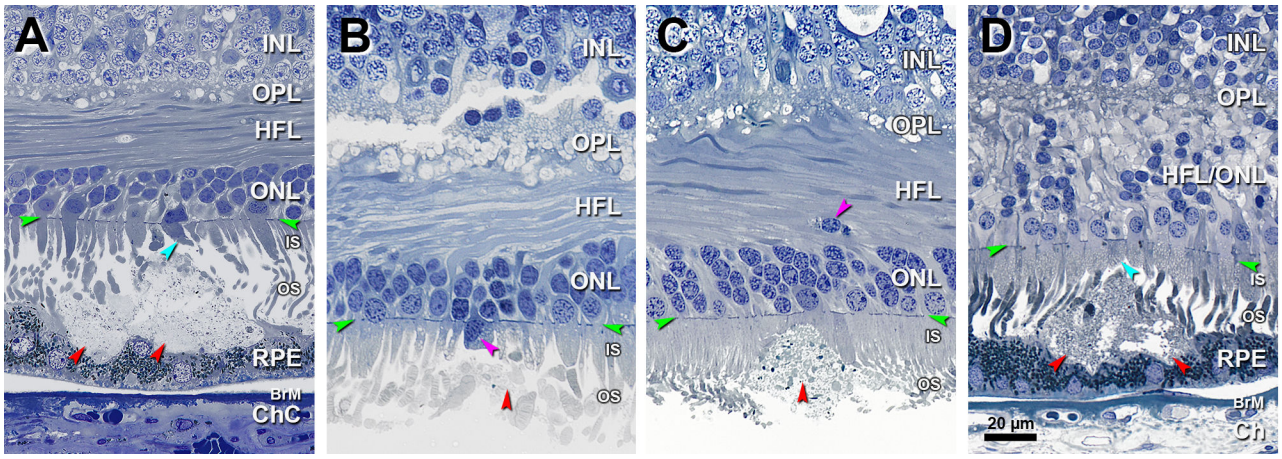

Figure 3. Solitary SDD protrude into overlying inner segments.

INL, inner nuclear layer; OPL, outer plexiform layer; HFL, Henle fiber layer; ONL, outer nuclear layer; IS, inner segment; OS, outer segment; RPE, retinal pigment epithelium; BrM, Bruch membrane; Ch, choroid; Green arrowheads, ELM, external limiting membrane. Red arrowheads, SDD, subretinal drusenoid deposits. Scale bar in (D) applies to all panels. SDD are artifactually split in B,C. **A.** 1400 µm temporal. A large SDD indents the apical surface of RPE. Photoreceptor OS fragments form a cap on the SDD surface, and overlying IS are short (teal arrowhead). Eighty-five-year-old woman. **B.** 1800 µm nasal. SDD fragments, absent photoreceptor OS, and short IS, one with an ectopic nucleus (purple arrowhead). Eighty-five-year-old woman. **C.** 850 µm nasal. SDD bulges into photoreceptor IS. Deposit contains heterogeneous debris including a few melanosomes. Photoreceptors OS disappear and IS are short over the deposit apex. Ectopic photoreceptor nuclei (an early indication of dyslamination) localize to the HFL (purple arrowhead). Eighty-eight-year-old man. **D.** 1900 µm nasal. SDD mound makes wavy concavities in the RPE surface that result in a thinned but still intact layer. Photoreceptor OS, recognized by presence of disks, are found within SDD, underlying short IS (teal arrowhead). Dyslamination of HFL and ONL is apparent. Seventy-six-year-old woman.

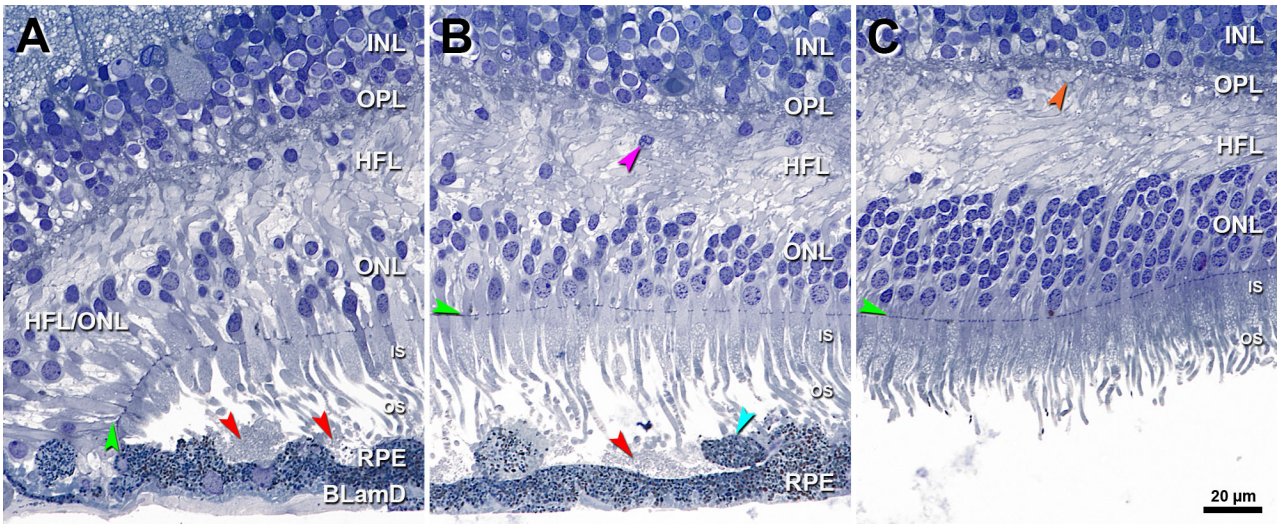

Figure 4. Border of geographic atrophy with subretinal drusenoid deposits.

INL, inner nuclear layer; OPL, outer plexiform layer; HFL, Henle fiber layer; ONL, outer nuclear layer; IS, inner segment; OS, outer segment; RPE, retinal pigment epithelium; BLamD, basal laminar deposit; Green arrowheads, ELM, external limiting membrane. Red arrowheads, SDD, subretinal drusenoid deposits; Scale bar in (C) applies to all panels. **A.** 1500 µm temporal. The ELM descent is a curved line that delineates the border of atrophy signified by OS absence and IS shortening at the descent. SDD are set back from this border on a wavy but intact RPE layer. The HFL and ONL is dyslaminate, and the HFL is disordered. **B.** 150 µm temporal to the ELM descent, SDD are observed, with sloughed RPE (teal arrowhead) and longer photoreceptors than in A. In the overlying ONL and HFL are several ectopic nuclei (purple arrowhead). **C.** 400 µm temporal to ELM descent, the HFL is disordered with only one ectopic nucleus. Cone pedicles with dark staining synaptic complexes (orange arrowhead) indicate good tissue fixation quality. OS were artifactually detached from the RPE. Seventy-six-year-old woman.

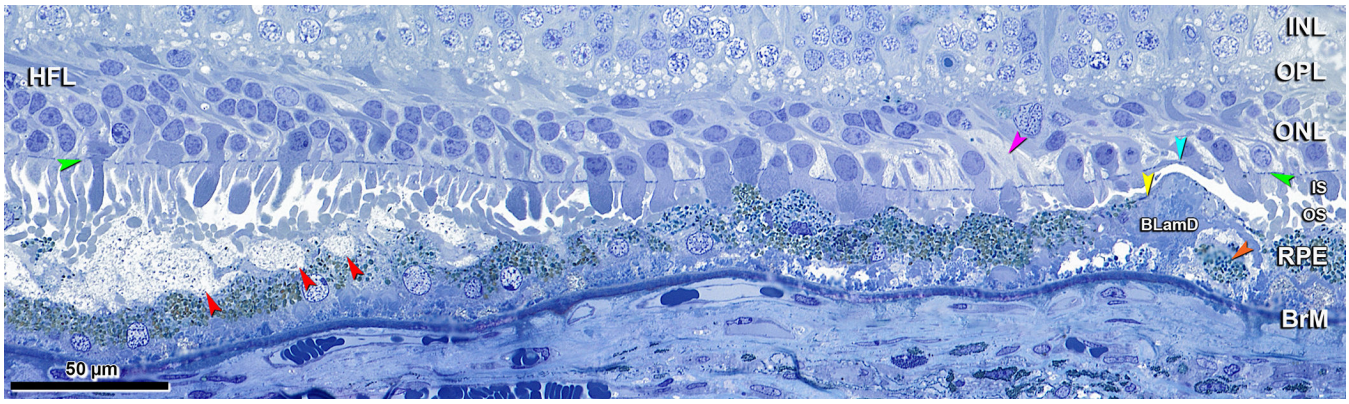

Figure 5. Transition from subretinal drusenoid deposits to outer retinal atrophy.

INL, inner nuclear layer; OPL, outer plexiform layer; HFL, Henle fiber layer; ONL, outer nuclear layer; IS, inner segment; OS, outer segment; RPE, retinal pigment epithelium; BrM, Bruch membrane; BLamD, basal laminar deposit; Green arrowheads, ELM, external limiting membrane; Red arrowheads, SDD, subretinal drusenoid deposits. **A.** 2300 µm nasal. From left to right (less affected to more affected) SDD diminish in size in association with photoreceptor OS displacement, IS shortening and ONL thinning. Thickness of RPE and BLamD varies little across this area. The area with SDD gradually transitions to an area lacking SDD and photoreceptor OS and IS are short. Further to the right, gaps in the ONL due to photoreceptor loss are filled with pale-staining hypertrophic Müller cells (purple arrowhead). The RPE is relatively intact over continuous BLamD which thickens and includes basal mounds. At the right is local RPE atrophy (yellow arrowhead) with persistent BLamD, shedding of RPE granule aggregates (orange arrowhead) into the basal mound, and slight upward deflection of the ELM (teal arrowhead). Eighty-five-year-old woman.

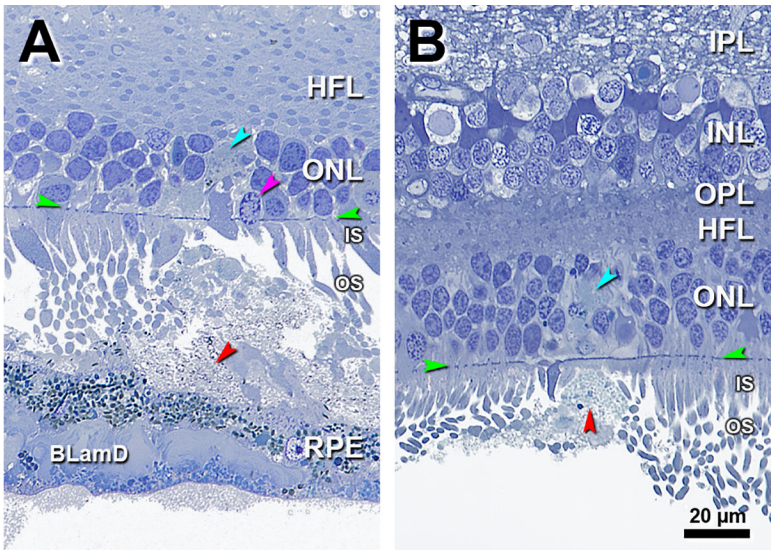

Figure 6. Subretinal drusenoid deposit material in the ONL.

IPL, inner plexiform layer; INL, inner nuclear layer; OPL, outer plexiform layer; HFL, Henle fiber layer; ONL, outer nuclear layer; IS, inner segment; OS, outer segment; RPE, retinal pigment epithelium; BrM, Bruch membrane; Ch, choroid; BLamD, basal laminar deposits. Green arrowheads, ELM, external limiting membrane. Red arrowheads, SDD, subretinal drusenoid deposits; Scale bar in (B) applies to all panels. **A.** 1300 µm temporal. SDD materials are interspersed among photoreceptors with an ONL gap (teal arrowhead) possibly indicating SDD material or disorganized cell processes. Photoreceptors IS are shortened and deflected, and one photoreceptor nucleus is displaced to IS (purple arrowhead). RPE with thick BLamD overlies soft druse with partial contents due to detachment. Eighty-five-year-old woman. **B.** 2500 µm temporal. SDD closely approximates the ELM, and a blue stained gap in the ONL (teal arrowhead) may represent SDD material or disorganized cell processes. OS disappear and IS are very short. The SDD apex detached from the base. Eighty-three-year-old woman.

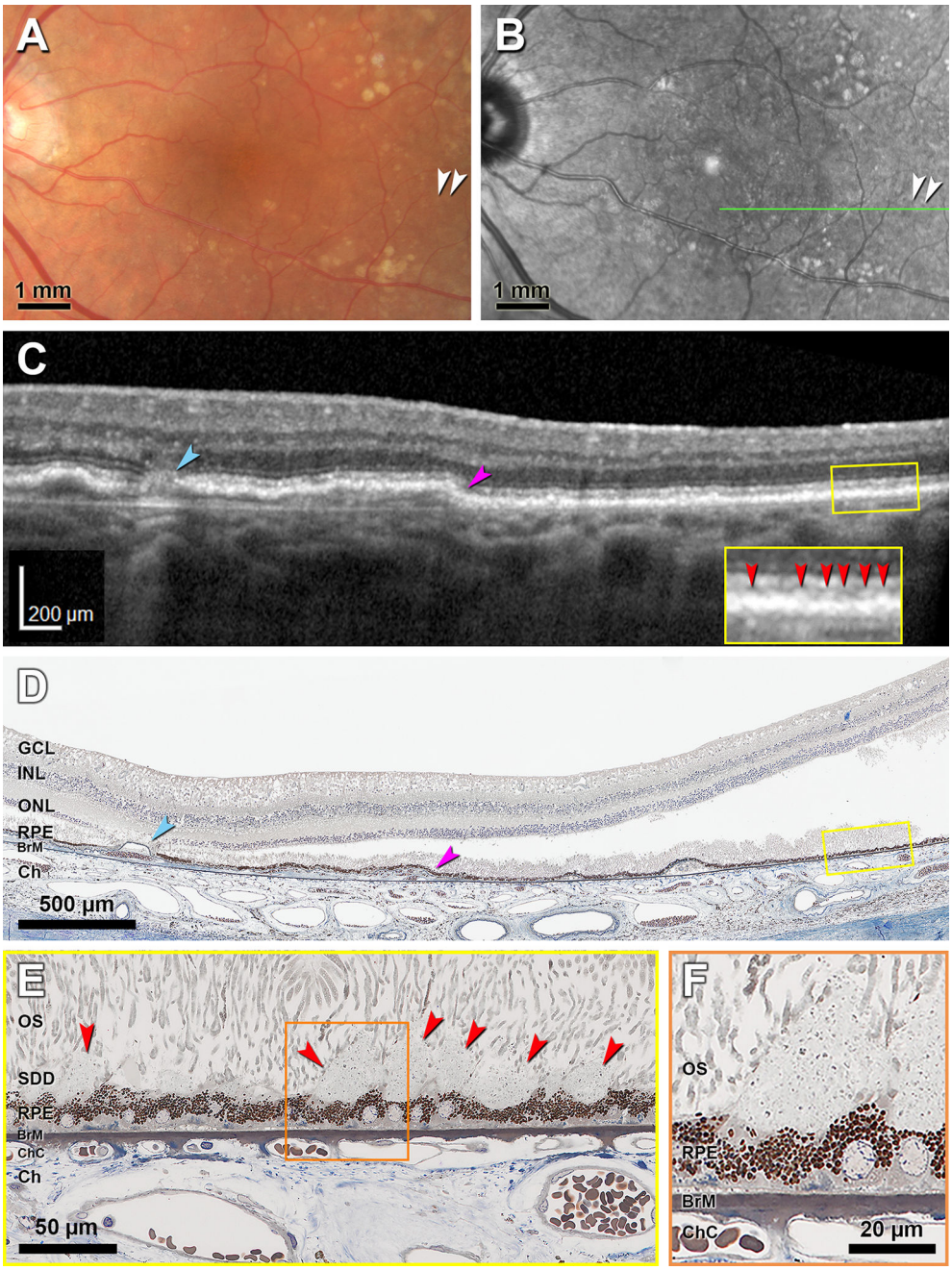

Figure 7. Clinicopathologic correlation of stage 1 subretinal drusenoid deposit in a neovascular AMD eye.

CFP, color fundus photograph; OCT, Optical coherence tomography. GCL, ganglion cell layer; INL, inner nuclear layer; ONL, outer nuclear layer; OS, outer segment; RPE, retinal pigment epithelium; BrM, Bruch membrane; ChC, choriocapillaris; Ch, choroid; SDD, subretinal drusenoid deposits; Green arrowheads, ELM, external limiting membrane. Red arrowheads, SDD. **A.** CFP shows accumulation of light-yellow materials that are not well delineated (white arrowheads). **B.** Near infrared reflectance shows hyporeflective dot SDD (white arrowheads). **C.** OCT B-scan at the location of green line in panel B shows an

atrophic spot (teal arrowhead) and an extensive shallow RPE elevation (purple arrowhead). Furthermore, groups of hyperreflective SDD are situated between Ellipsoid zone and RPE (red arrowheads in yellow inset). **D.** Histologic image shows the atrophic spot (teal arrowhead) and RPE elevation (purple arrowhead), thus establishing correspondence with the OCT B-scan. Yellow frame shows a region with SDD magnified in (E). Artifactual bacillary layer detachment is apparent. **E.** Several SDD above scalloped RPE (red arrowheads) correspond exactly with the hyperreflective deposits seen in OCT. Photoreceptor OS are deflected by the SDD. Shed OS are visible on the surface of SDD. Orange frame shows SDD magnified in (F). **F.** SDD internal structure consists of finely granular material within a flocculent ground substance. Ninety-year-old woman.

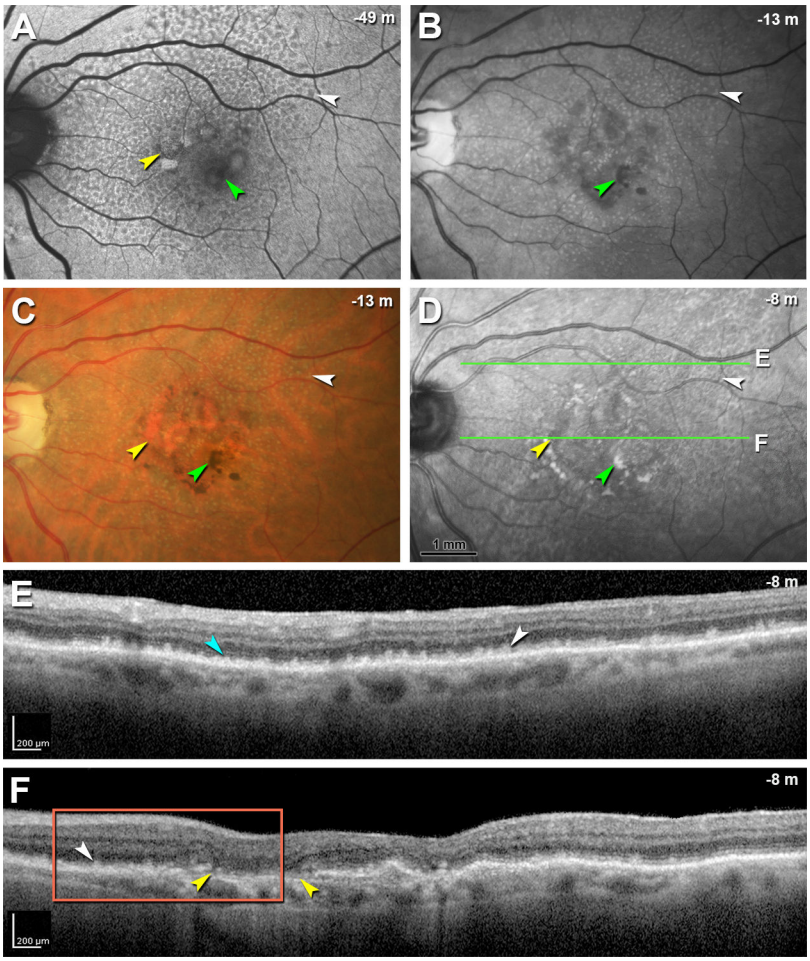

Figure 8. Multimodal imaging of stage 2 and stage 3 subretinal drusenoid deposit in transition to outer retinal atrophy.

SDD, subretinal drusenoid deposit; RPE, retinal pigment epithelium; ELM, external limiting membrane; FAF, fundus autofluorescence; CFP, color fundus photograph; OCT, Optical coherence tomography. Image capture date is expressed as time before death in negative months. White arrowhead in A-D shows the same deposit in each modality. **A.** FAF shows multiple hyperautofluorescent vitelliform lesions (yellow arrowhead) with hyperpigmentation (green arrowhead) and many hypoautofluorescent dot SDD. **B.** Red free image shows hyperpigmentation (green arrowhead) and multiple dot SDD. **C.** CFP shows geographic atrophy (yellow arrowhead) with hyperpigmentation (green arrowhead) and many dot SDD. **D.** Near infrared reflectance shows hyporeflectivity of atrophic area (yellow arrowhead) with hyperpigmentation (green arrowhead) and, superior to the macula, dot SDD. Green lines indicate position of OCT B-scans in panels E and F. **E.** OCT B-scan at line E in panel D shows numerous highly reflective deposits that elevate (stage 2, teal arrowhead) or penetrate (stage 3, white arrowhead) the EZ. Disintegrating Type 3 deposits are accompanied by loss of outer retinal architecture and visualized EZ, plus thinning of the ONL. **F.** OCT B-scan at the location of line F in panel D shows reflective deposits (white arrowhead) close to the atrophic area (yellow arrowheads). Non-visibility of ELM, EZ, and

IZ signifies that this eye is transitioning to outer retinal atrophy. Orange frame shows site of histology in Figure 9B. Nighty-eight-year-old woman with advanced AMD.

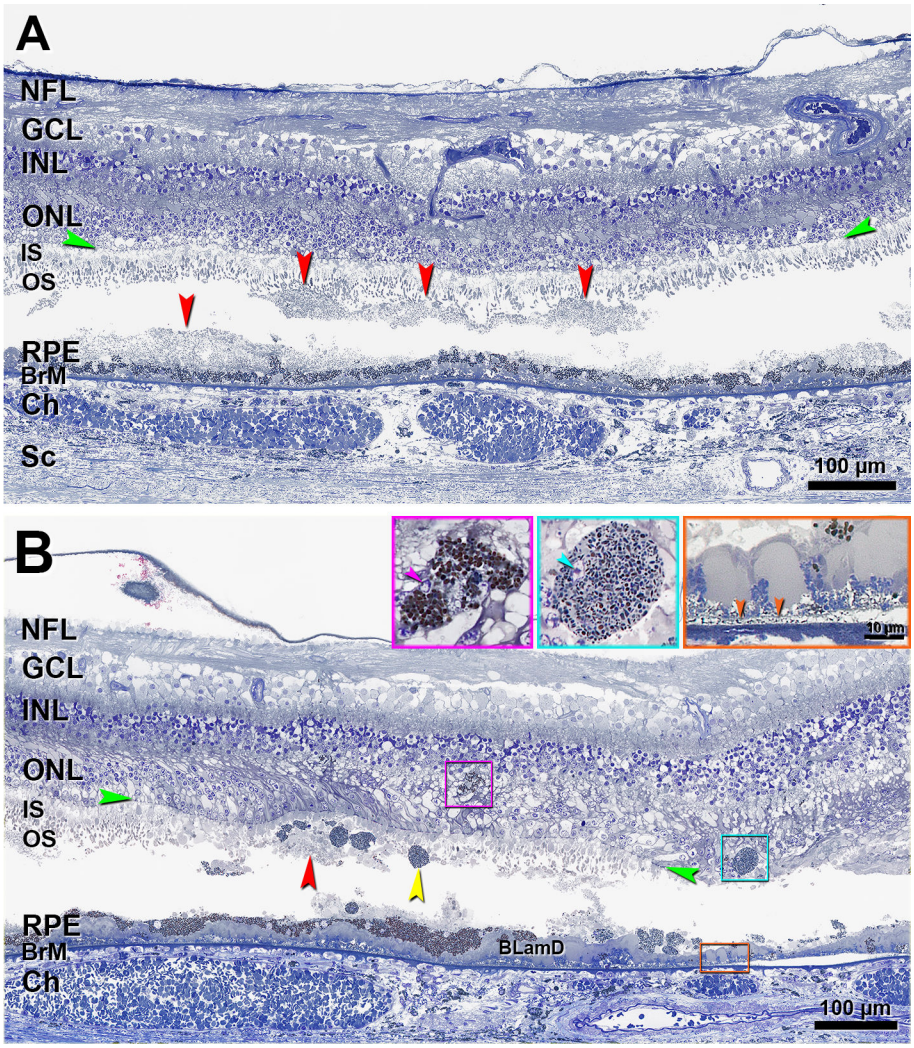

Figure 9. Histology of stages 2–3 subretinal drusenoid deposit in an eye with geographic atrophy and incipient outer retinal atrophy.

Histology comes from the patient in Figure 8. NFL, nerve fiber layer; GCL, ganglion cell layer; INL, inner nuclear layer; ONL, outer nuclear layer; IS, inner segment; OS, outer segment; RPE, retinal pigment epithelium; BrM, Bruch membrane; Ch, choroid; Sc, sclera; BLamD, basal laminar deposit; Green arrowheads, ELM, external limiting membrane. Red arrowheads, SDD, subretinal drusenoid deposits; Scale bar in the aqua inset also applies to the purple inset. In both panels, SDD split and contents were partially lost. **A.** The undulating nature of these SDD is well visualized. Photoreceptor OS are affected but IS are intact (stage 2 SDD). **B.** In the same region as the orange frame in Figure 8F, SDD fragments can be observed in the sub-retinal space. Photoreceptor OS disappear, IS are very short, sloughed RPE (yellow arrowhead) is present exactly at the stage 3 SDD. Two intraretinal RPE cells with different shapes and internal contents can be observed (purple and aqua frames and insets). The purple inset shows the same cell in another section in this series. This cell has an irregular shape and a small nuclear profile (arrowhead); pigment granules inside this cell are similar in size and color to cells in the RPE layer. The cell in the aqua inset is ovoid, and it has a small nucleus (arrowhead) and its pigment granules are

smaller and less densely packed than those in the RPE layer. At the right is geographic atrophy (Figure 8C,F), with thick BLamD, and delimited by an ELM descent (green arrowheads). Of the atrophic area, a 300 μm length is shown, and 110 μm is off the right edge. BLinD is a gray thin layer continuous with an area of RPE-BLamD detachment from Bruch's membrane (orange frame and inset, orange arrowheads).

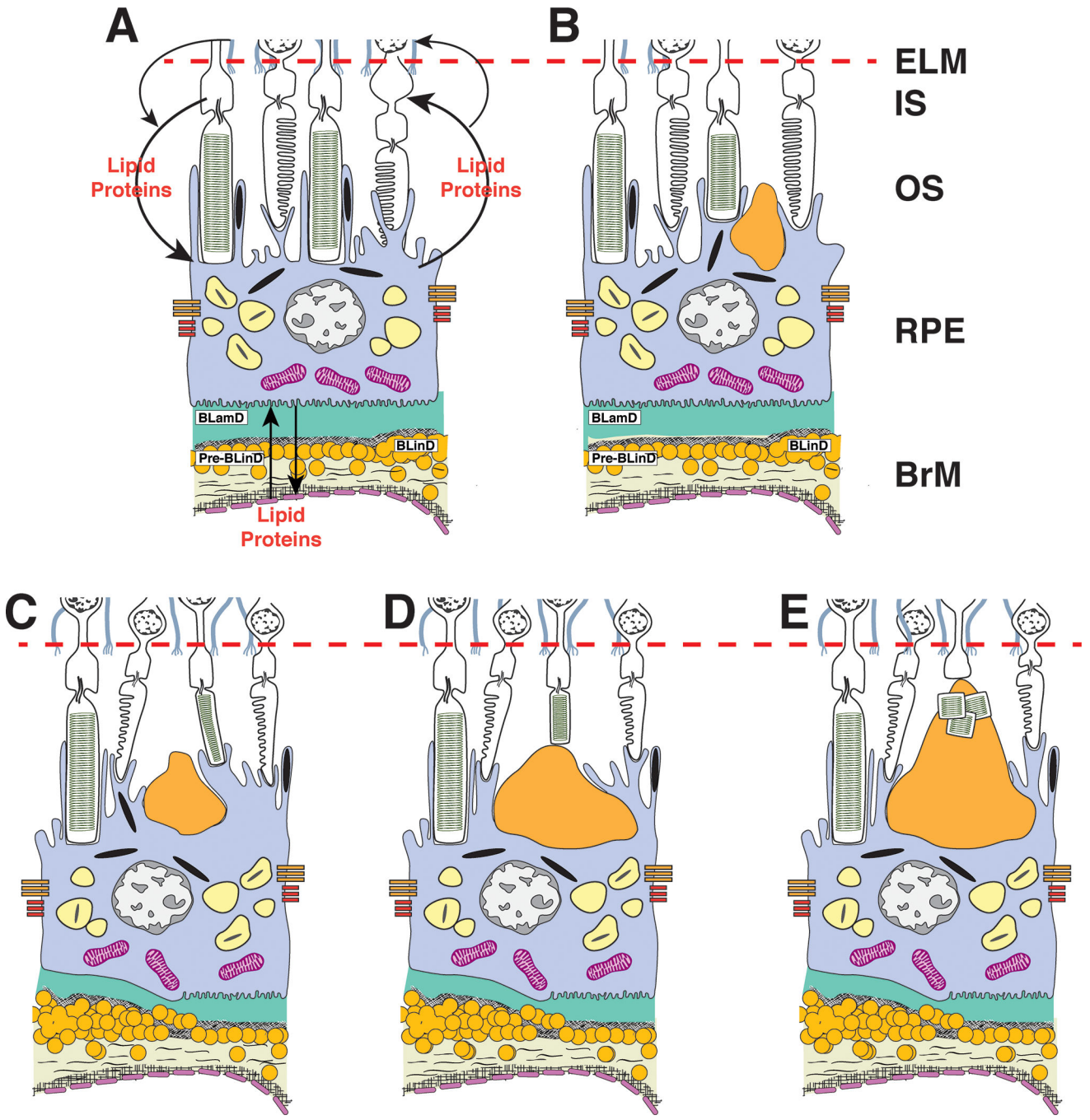

Figure 10. Initiation and growth of subretinal drusenoid deposits

ELM, external limiting membrane; IS, inner segments; OS, outer segments; RPE, retinal pigment epithelium; BrM, Bruch's membrane. **A.** We envision a physiologic cycling of lipids (e.g., cholesterol, fatty acids, retinoids, xanthophyll carotenoids) and carrier/ transfer proteins (e.g., apolipoprotein E, interphotoreceptor binding protein) among the circulation, RPE, photoreceptors, Müller glia, and back again (arrows; details available[7, 77]) **B.** The smallest SDD (before clinical stage 1) are found at the RPE, suggesting that they start there. **C,D,E.** We hypothesize that deposits grow from the top, as clinical stages progress.

Histologic data suggest a molecular blockage at the RPE (e.g., reduced capacity to bind cycled molecules) leading to accumulated materials. Once begun, a deposit seeds subsequent physical accumulation towards the ELM (including OS fragments when deposits are large). Photoreceptors focally deflect and shorten. Deposit constituents are cleared by Müller glia without glial scar formation.